Numerical Investigation of the Inner Profiles of Ironmaking Blast Furnaces: Effect of Throat-to-Belly Diameter Ratio

ZHAOYANG LI, SHIBO KUANG, DINGLIU YAN, YUANHONG QI, and AIBING YU

The inner profile of iron making blast furnace (BF) is of significant importance to reactor performance. However, its determination lacks any sound theoretical and empirical base. This paper presents a numerical study of the multiphase flow and thermochemical behaviors inside BFs with different inner profiles by a multi-fluid process model. The validity of the model is first confirmed by various applications. It is then used to study the effect of throat-to-belly diameter ratio (R_D) with respect to productivity, burden distribution pattern, and softening-melting temperature of ferrous materials. The results show that when R_D increases, the fuel rate increases at relatively low productivities; however, it initially decreases to a minimum and then increases at relatively high productivities. This performance against R_D to some degree varies with either burden distribution pattern or softening-melting temperature of ferrous materials. Optimum R_D can be identified with relatively small coke rate and minimum fluctuations of global performance and in-furnace states. The analysis of the in-furnace states reveals that the flow and thermochemical behaviors above the cohesive zone are drastically deteriorated with increasing productivity for BFs with relatively small R_D, leading to different variation trends of fuel rate.

DOI: 10.1007/s11663-016-0831-6
© The Minerals, Metals & Materials Society and ASM International 2016

I. INTRODUCTION

BLAST furnace (BF) ironmaking is the most important technology by which hot metal (HM) is continuously and rapidly reduced from iron-bearing materials. This process accounts for over 96 percent of the total HM production for steelmaking in the world.[1] It is recognized that in order to achieve high-level performance, BF inner profile or geometry has to meet the physical and chemical requirements of counter-, co-, and/or cross-current flows of descending solids and liquid as well as ascending gas over the region from the hearth to the top.[2] However, because of the complexity of BF, it is extremely difficult if not impossible to measure the details of inner flow and thermochemical phenomena and then consider them at the design phase. Consequently, for a long time, the inner profile has evolved through experience, of which the calculation is more or less empirical.[2] Moreover, such calculation cannot fully take into account the effects of operational condition, material property, and their variations. However, these effects are very useful for obtaining an optimum inner profile and for avoiding possible rapid changes of BF inner states with varying material and/or operational conditions. Additionally, the problem associated with determination of BF geometry can become more serous by the uncertainties from the implementation of new technologies. Therefore, with either a short-term or long-term view, there are needs to reveal the effects of furnace profiles under different conditions, particularly at a quantitative level.

In the past years, various experimental studies have been conducted to study the effects of BF inner profiles.[3-6] Although useful to better know the impact of furnace profile, the previous studies were mainly based on scaled-down cold models and largely confined to the visual observation of particle flow patterns. In fact, at this stage of development, it is yet difficult to measure the local solid structures, multiphase flows, and related phenomena which are critical for understanding BFs and other particle-fluid systems.[7-9] Moreover, real BFs are operated under extremely harsh environment, involving intensive interactions among gas, solid, and liquid in terms of flow, and heat and mass transfer at high temperature and pressure. They are therefore not easy to simulate experimentally. This problem may, to some extent, be overcome by a small experimental BF (*e.g.*, 9-m^3 LKAB BF[10]), which in principle functions in a similar way to a real BF. However, it is unaffordable to build up, run, and maintain such an experimental platform for most investigators, especially when a number of furnaces are needed to examine the effect of inner profile. Moreover, the scale-up issue from experimental BFs to industrial ones has not been fully resolved yet.

ZHAOYANG LI, Ph.D. Candidate, SHIBO KUANG, Research Fellow, and AIBING YU, Professor, are with the Laboratory for Simulation and Modelling of Particulate Systems, Department of Chemical Engineering, Monash University, Clayton, Melbourne, VIC 3800, Australia. Contact e-mail: shibo.kuang@monash.edu DINGLIU YAN and YUANHONG QI, Professors, are with the State Key Laboratory for Advanced Iron and Steel Processes and Products, Central Iron and Steel Research Institute, Beijing 100081, China.

Manuscript submitted June 15, 2016.
Article published online October 17, 2016.

Table I. Governing Equations of the Present Model

Items	Description
Mass conservation	$\nabla \cdot (\varepsilon_i \rho_i \mathbf{u}_i) = S_i$, where $S_i = -\sum_k \beta_{i,k} R_k^*$
Momentum conservation	
Gas	$\nabla \cdot (\varepsilon_g \rho_g \mathbf{u}_g \mathbf{u}_g) = \nabla \cdot \boldsymbol{\tau}_g - \varepsilon_g \nabla p + \rho_g \varepsilon_g \mathbf{g} + \mathbf{F}_g^s$
	$\boldsymbol{\tau}_g = \varepsilon_g \mu_g [\nabla \mathbf{u}_g + (\nabla \mathbf{u}_g)^T] - \frac{2}{3} \varepsilon_g \mu_g (\nabla \cdot \mathbf{u}_g) \mathbf{I}$
Solid	$\nabla \cdot (\varepsilon_s \rho_s \mathbf{u}_s \mathbf{u}_s) = \nabla \cdot \boldsymbol{\tau}_s - \varepsilon_s \nabla p_s + \rho_s \varepsilon_s \mathbf{g}$
	$\boldsymbol{\tau}_s = \varepsilon_s \mu_s [\nabla \mathbf{u}_s + (\nabla \mathbf{u}_s)^T] - \frac{2}{3} \varepsilon_s \mu_s (\nabla \cdot \mathbf{u}_s) \mathbf{I}$
Liquid	$v_l = const,\ u_l = 0$
Heat and species conservation	$\nabla \cdot (\varepsilon_i \rho_i \mathbf{u}_i \varphi_{i,m}) - \nabla \cdot (\varepsilon_i \Gamma_i \nabla \varphi_{i,m}) = S_{\phi_{i,m}}$
	if $\varphi_{i,m}$ is $H_{i,m}$, $\Gamma_i = \frac{k_i}{c_{p,i}}$
	$S_{\varphi_{i,m}} = \delta_i h_{ij} \alpha (T_i - T_j) + \eta_i \sum_k R_k^* (-\Delta H_k)$
	If $\varphi_{i,m}$ is $\omega_{i,m}$, $\Gamma_i = \rho_i D_i$, $S_{\phi_{i,m}} = \sum_k \alpha_{i,m,k} R_k^*$,
	where $\varphi_{i,m} = \omega_{g,CO}, \omega_{g,CO_2}, \omega_{g,H_2}, \omega_{g,H_2O}, \omega_{g,N_2}, \omega_{s,Fe_2O_3}, \omega_{s,Fe_3O_4}, \omega_{s,FeO}, \omega_{s,flux}$
Phase volume fraction	$\sum_i \varepsilon_i = 1$
State equation	$p = \sum_i (y_i M_i) R T_g / V_g$

On the other hand, computer modeling and simulation has been recognized as promising to overcome the deficiencies associated with the experimental studies. It has been widely used to study localized or global particulate and multiphase flow and thermochemical behaviors inside BFs under different conditions (see, *e.g.*, the reviews by different investigators[7,11-13]). Generally speaking, the existing approaches can be discrete- or continuum-based with respect to the solid phase, which are represented by discrete element model (DEM) and two-fluid (or multi-fluid) model (TFM), respectively.[14] To date, the DEM studies of furnace profiles have focused on the solid flows inside scaled-down BFs with respect to, for example, shaft and bosh angles,[15,16] BF volume,[17] and abnormal wall shape related to the scaffolding phenomenon.[18] However, DEM-based simulations are computationally too demanding to consider a real BF, where the number of particles can be billions. Moreover, such an approach is still under heavy developments toward fully describing the coupled multiphase flows and their thermochemical behaviors inside BFs, although some encouraging progress has been recently achieved.[19-22] The TFM approach has been better developed and extensively used to re-produce the primary phenomena related to gas, solid, liquid, and powder and thus global performance of full scale or real BFs. Some examples include the modeling of chemical reactions,[23] liquid flow in form of droplet/rivulet,[24-26] transient behaviors,[27] deadman,[28] layered structure of iron ore and coke,[29-31] and multi-phases.[32,33] Although the usefulness of the process models resulting from these developments have been demonstrated through various applications,[7] to date the efforts dedicated to studying the effect of furnace profile by continuum models are few. Only two studies were reported thus far by Takatani *et al.*,[34,35] who, however, focused on the in-furnace stress states and provided the results confined to the effect of furnace profile on fuel rate under fixed operational and material conditions. To date, comprehensive studies of the inner states and global performance of BF against inner profiles cannot be found in the literature. Moreover, the quantitative effects of operational condition and raw material properties on determination of BF geometry are lacking. However, such information is highly desired to achieve the reliable and efficient running of BFs in practice.

In this work, the multi-fluid BF process model reported elsewhere[31,36] has been further developed, validated, and then used to study the effect of BF inner profile on the in-furnace flow and thermochemical behaviors as well as global performance. An important tendency in designing a modern BF is to achieve higher production capacity and process efficiency by adjusting the dimensions horizontally rather than vertically.[2,35] With this realization, all the inner profiles are done here by adjusting the lateral dimensions, with the heights of different parts fixed. Another important consideration coupled with BF geometry design is the change of productivity, which is achieved here mainly by varying blast rate over a wide range. Quantifying the effect of productivity under different furnace profiles can benefit determination of BF geometry for the sake of the following facts. First, BF performance somewhat varies with the change of productivity.[37,38] Second, BF productivity may need to be adjusted to adapt to the market needs, especially when the steel industry is going through its worst downturns. Besides the study of different productivities, the effects of

Table II. Chemical Reactions and Transport Coefficients in the Present Model

	Terms	Formulation
Reactions	$Fe_2O_{3(s)} + CO_{(g)} = Fe_{(s)} + CO_{2(g)}$[46]	$R_1^* = 12\xi_{\text{ore}}\varepsilon_{\text{ore}}P(y_{CO} - y_{CO}^*)/(8.314T_s)/$ $\{d_{\text{ore}}^2/D_{g,CO}^e[(1-f_0)^{-1/3} - 1] + d_{ore}[k_1(1+1/K_1)]^{-1}\}$
	$FeO_{(l)} + C_{(s)} = Fe_{(l)} + CO_{(g)}$[47]	$R_2^* = k_2\frac{A_c}{V_b}\alpha_{FeO}, \frac{A_c}{V_b} = 0.468[\varepsilon\phi_{\text{coke}}d_{coke}]$
	$C_{(s)} + CO_{2(g)} = 2CO_{(g)}$[46]	$R_3^* = \frac{6\xi_{\text{coke}}\varepsilon_{\text{coke}}py_{co_2}/(8.314T_s)}{d_{\text{coke}}/k_f + 6/(\rho_{\text{coke}}E_f k_3)}$
	$FeO_{(s)} \rightarrow FeO_{(l)}$[23]	$R_4^* = \left\langle \frac{T_i - T_{\min,sm}}{T_{\max,sm} - T_{\min,sm}} \right\rangle_0^1 \frac{\oint \omega_{sm}\mathbf{u}_i\rho_i\varepsilon_i dA}{M_{sm}Vol_{cell}}$
	$Flux_{(s)} \rightarrow Slag_{(l)}$	
	$Fe_2O_{3(s)} + H_{2(g)} = Fe_{(s)} + H_2O_{(g)}$[46]	$R_5^* = (\pi \cdot d_{\text{ore}}^2\varphi_{ore}^{-1}N_{ore} \cdot 273 \cdot P(y_{H_2} - y_{H_2}^*)/(22.4T_{\text{solid}}))/\{1/k_{f5}$ $+(d_{\text{ore}}/2)[(1-f_s)^{-1/3} - 1]D_{s5} + [(1-f_s)^{2/3}k_5(1+1/K_5)]^{-1}\}$
	$C_{(s)} + H_2O_{(g)} = CO_{(g)} + H_{2(g)}$[46]	$R_6^* = (\pi d_{coke}^2\varphi_{\text{coke}}^{-1}N_{\text{coke}} \cdot 273 \cdot Py_{H_2O}/22.4T_{\text{solid}})$ $/(1/k_{f6} + 6/d_{\text{cokre}}\rho_{\text{coke}}E_f' k_6)$
	$CO_{(g)} + H_2O_{(g)} = CO_{2(g)} + H_{2(g)}$[47]	$R_7^* = 7.29 \times 10^{11}(y_{CO})^{1/2}(y_{H_2O})(P/T_{\text{gas}})^{3/2}\varepsilon\frac{\exp(-67300/RT_{\text{gas}})}{\sqrt{1 + 14.158y_{H2}PT_{\text{gas}}}}$ $- 1.386 \times 10^{10}(y_{CO})(y_{H2})^{1/2}(P/T_{gas})^{3/2}\varepsilon\frac{\exp(-57000/RT_{\text{gas}})}{\sqrt{1 + 4.24y_{CO}PT_{\text{gas}}}}$
	$SiO_{2(l)} + 2C = Si + 2CO_{(g)}$	$R_8^* = k_8(A_v/V_B)C_{SiO_2}$
	$SiO_{2(l)} + 2C_{(l)} = Si_{(l)} + 2CO_{(g)}$[47]	$k_8 = 7.59 \times 10^4\exp(-62870/RT_s)$
Diffusion	Gas[47]	$\text{Re}_g \geq 8; Pe_{gx} = 8, Pe_{gy} = 2.0$ $\text{Re}_g < 8; Pe_{gx} = \text{Re}_g, Pe_{gy} = 0.25\text{Re}_g$
Conductivity	Gas[47]	$k_{gn} = C_p\rho D_{gn}^e \;\; R_3^* = \frac{6\xi_{\text{coke}}\varepsilon_{\text{coke}}py_{co_2}/(8.314T_s)}{d_{\text{coke}}/k_f + 6/(\rho_{\text{coke}}E_f k_3)}$
	Solid[47]	$k_{se}^e = (1-\varepsilon_g)/[(1/k_s + 1/k_s^e) + \varepsilon_g k_s^e] \;\; k_s^e = 2.29 \times 10^{-7}d_s T_s^3$
	Liquid[33]	$k_l = 0.0158T_l$ for HM $k_l = 0.57$ for slag
Heat transfer coefficients	Gas-solid[31]	$Nu = 2.0 + 0.6(\text{Pr})^{0.333}(\text{Re}_g)^{0.5}$
		$h_{gs} = 0.3h_{gs}^e, h_{gs}^e = Nuk_g/d_s$
	Gas-liquid[23]	$h_{g-slab} = (0.203\text{Re}_g^{0.33}\,\text{Pr}^{0.33} + 0.220\text{Re}_g^{0.5}\,\text{Pr}^{0.4})k_g/d_s$ $E_{gl} = 4.18 \times 10^{-4}\varepsilon_g\rho_g u_g C_{pg}(\varepsilon_l\rho_l u_l)^{0.35}\text{Re}_{gl}^{-0.37}$ $\cdot(Sc_g/\text{Pr}_g)^{0.667}(T_l - T_g)$
	Solid-liquid[23]	$h_{sl} = 1/(1/h_s + 1/h_l), h_s = 2\sqrt{k_s C_{ps}\rho_s\lvert\tilde{u}_l - \tilde{u}_s\rvert/\pi d_s}$ $h_l = \frac{k_l}{d_s}2\sqrt{\text{Re}_{sl}\,\text{Pr}_l}/(1.55\sqrt{\text{Pr}_l} + 3.09\sqrt{0.372 - 0.15\,\text{Pr}_l})$ where $\text{Re}_{sl} = \varphi_s d_s\rho_l\lvert\tilde{u}_l - \tilde{u}_s\rvert/\mu_l$ and $\text{Pr}_l = C_{pl}\mu_l/k_l$

burden distribution pattern and softening-melting property of ferrous materials on the determination of BF geometry are also examined considering the importance of top control in the routine operations. The results from this study can be useful for establishing a comprehensive picture of the in-furnace states and global performance of BFs against different inner profiles in relation to the changes of operational and material conditions.

II. MODEL DESCRIPTION

The present mathematical model is a steady-state, axisymmetric multi-fluid model, developed from the two-dimensional slot model reported elsewhere.[31,36] It considers the region of a BF from the slag surface in the hearth to the burden surface in the throat. The phases considered are gas, solid, hot metal (HM), and slag. They consist of one or more components and each

Table III. Geometrical Parameters of the BFs Simulated

Parameter	Present BF	LKAB BF
Hearth diameter (m)	10.6	1.2
Belly diameter (m)	13.1 (16.09-12.22)	1.6
Throat diameter (m)	7.96 (3.63-9.05)	1.0
Hearth height (m)	4.8	1.87
Bosh height (m)	3.2	0.86
Belly height (m)	1.0	0.31
Shaft height (m)	14.6	4.45
Throat height (m)	2.4	10.70
Bosh angle (deg)	68.66	76.90
Shaft angle(deg)	80.02	86.11
Useful height (m)	26	8.11
Useful volume (m^3)	2328.73	9.0

NB: Base case with varying ranges in the bracket.

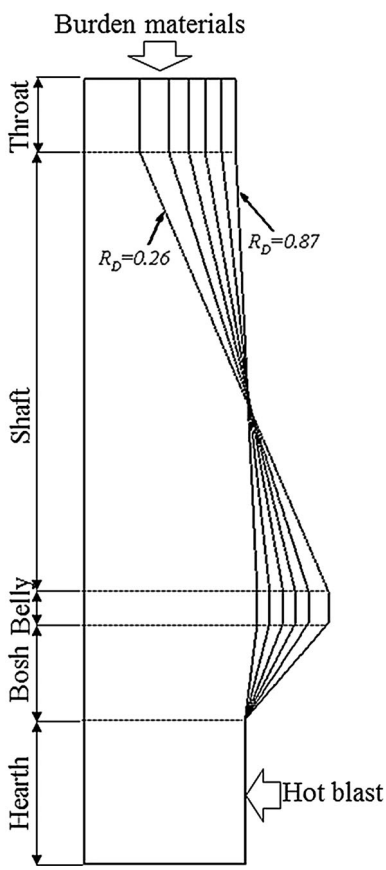

Fig. 1—Furnace profiles simulated in this study.

component has its own composition and physical properties. Each phase is described by separate conservation equations of mass, momentum, and enthalpy, with the key chemical reactions considered. The governing equations, chemical reactions, and transfer coefficients are summarized in Tables I and II.

The model is in principle similar to other BF process models developed by different investigators;[23,30,32-35] however, it is integrated with our recent efforts in the modeling of layered burden structures[31] as well as the variation of stockline.[36] The details of the model and relevant numerical techniques can be found elsewhere[23-25,28,31,33,36] and are not included in this paper for brevity.

III. SIMULATION CONDITIONS

Table III lists the dimensions of the BFs considered in the present study. Here, all the inner profiles are obtained at the same inner volume as that of the base BF used elsewhere.[36] This configuration aims to find an answer to the frequently asked question "how to determine a BF profile for a given volume." Provided that the inner volumes of different BFs are nearly the same, their hearth volumes generally do not change much.[35] Additionally, longitudinal dimensions such as the lengths of shaft, bosh, and throat do not change much according to the statistical data on typical BFs used in Japan.[34] In light of the above facts, the heights of the throat, shaft, belly, bosh, and hearth as well as the hearth diameter are fixed in this work. As such, the geometrical variables are only the throat and belly diameters. At a fixed inner volume, the two variables are correlated with each other and can be expressed as one, that is, throat-to-belly diameter ratio (R_D). In this study, the values of R_D are varied from 0.26 to 0.87, which correspond to the furnace profiles shown in Figure 1. For the base BF profile, the value of R_D is equal to 0.62.

The simulated operational and material conditions follow our previous studies,[31,36] as listed in Table IV. In practice, an increased productivity can be achieved by increasing oxygen supply through increased blast volume or rate, oxygenated blast, humidified blast, and high top pressure.[2] In this study, to consider the effect of inner profile over a wide range of productivities, the flow rate of hot blast (W_b) is treated as another variable. Assuming that blown-in blast can always be accepted by the BFs, it is changed from 3043 to 8700 Nm^3/min, with the composition and temperature fixed. Accordingly, different productivities are obtained as part of simulation outputs, which range from 1.61 to 3.98 for the base BF. Additionally, the burden distribution pattern at the BF top and softening-melting temperature of ferrous materials are varied to examine their impacts on the determination of BF geometry.

Based on the given hot blast conditions and coke properties, the composition, temperature, and flow rate of the reducing gas generated from the raceway are determined according to the local mass and heat balance, and used as the inlet conditions of gas phase in simulations, as done in almost all of the previous continuum modeling of BF process.[23,27,30,31,33-35] The burden materials containing iron ore, coke, and flux are charged onto the furnace from the top with an identical downward velocity. In all the simulations, in order to generate comparable results, the HM temperature at the slag surface remains constant, 1883 K (1610 °C), similar to the previous studies.[34,35,39-41] This is achieved by adjusting coke rate in each simulation when furnace profile, operational condition, or material properties are varied.

Table IV. Operational Conditions Considered in this Study

Variables	Present BF	LKAB BF
Gas phase		
Inlet velocity, m/s	56.1-160.4	81.4
Inlet gas component, mole percentage	34.959 pct CO; 0.0 pct CO_2; 0.813 pct H_2; 0.0Pct H_2O; 64.228 pct N_2	41.25 pct CO; 0.0 pct CO_2; 5.456 pct H_2; 5.3293 Pct H_2O;
Inlet gas temperature, K (°C)	2586.6 (2313.6)	2540 (2267)
Top pressure, atm	2.0	1.5
Solid phase		
Ore, t/tHM	1.64	1.733
Ore components, mass fraction	Fe_2O_3 0.6566; FeO 0.1576; CaO 0.0652; MgO 0.0243; SiO_2 0.06; Al_2O_3 0.0295; MnO 0.0061; P_2O_5 0.008	Fe_2O_3 0.6040; FeO 0.0923; CaO 0.0930; MgO 0.0143; SiO_2 0.0475; Al_2O_3 0.0123; MnO 0.003873; P_2O_5 0.000687
Average ore particle size, m	0.03	0.018
Coke, kg/tHM	500	450
Coke components, mass fraction	C 0.857; Ash 0.128; S 0.005; H 0.005, N 0.005	C 0.8576; Ash 0.1271; S 0.005; H 0.0933, N 0.0088
Average coke particle size, m	0.045	0.025
Flux, t/tHM	0.0264	0.0683
Flux components, mass fraction	CaO 0.438; MgO 0.079; SiO_2 0.024; Al_2O_3 0.033; CO_2 in CaO 0.344; CO_2 in MgO 0.082	CaO 0.438; MgO 0.079; SiO_2 0.024; Al_2O_3 0.033;CO_2 in CaO 0.344; CO_2 in MgO 0.082
Ore voidage	$0.403(100d_{ore})^{0.14}$	$0.403(100d_{ore})^{0.14}$
Coke voidage	$0.153\log d_{coke}+0.742$	$0.153\log d_{coke}+0.742$
Ore/(ore + coke) volumetric ratio	0.5923	0.528
Burden temperature, K (°C)	298 (25)	298 (25)

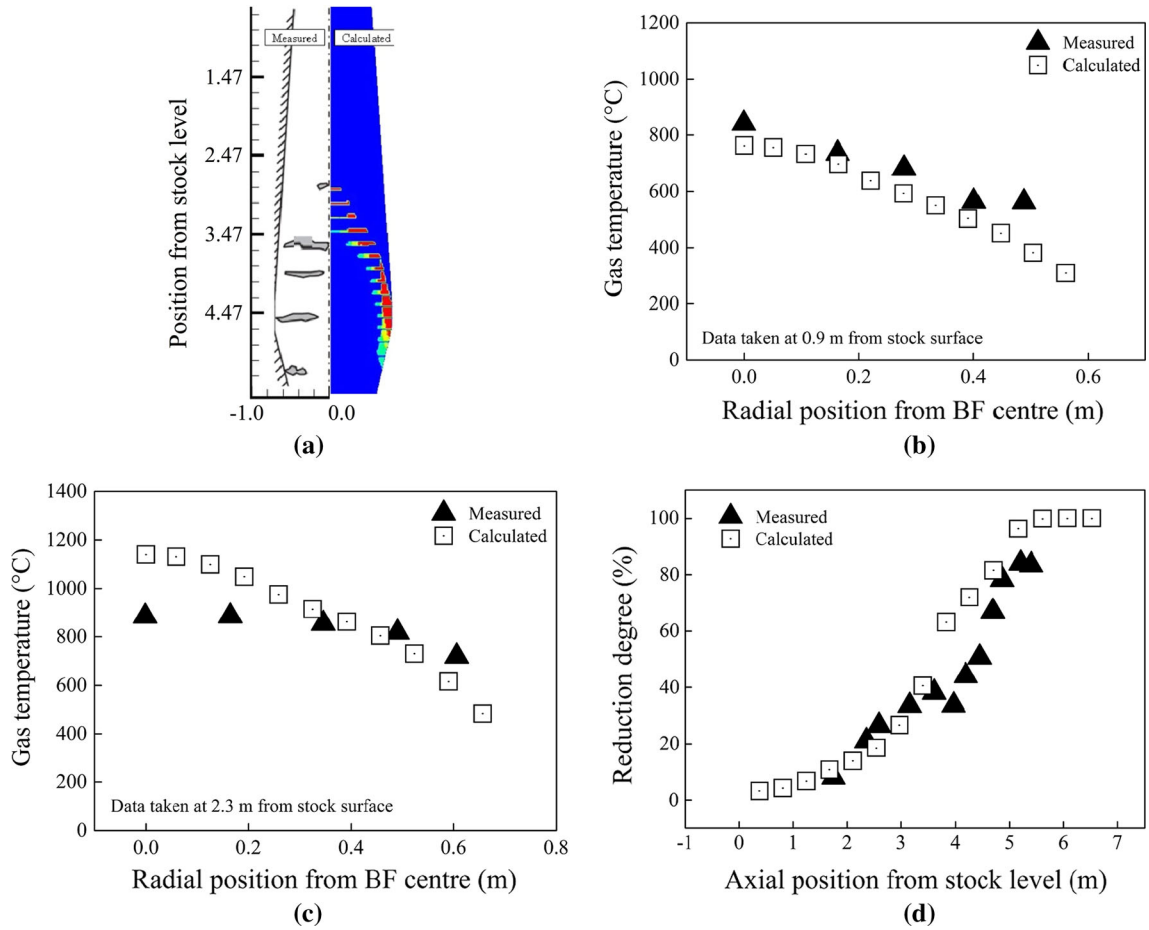

Fig. 2—Comparison of the calculated and measured results of LKAB BF in terms of: (*a*) CZ profile, (*b*) gas temperature at the upper probe, (*c*) gas temperature at the lower probe, and (*d*) reduction degree.

Table V. Comparison of Calculated and Measured Performance Indicators of LKAB BF

Variables	Unit	Measured	Calculated	Error (pct)
Adiabatic flame temperature	K (°C)	2419 (2218)	2540 (2267)	2.21
Top gas utilization factor	%	42.4	42.43	0.07
Top gas temperature	K (°C)	493 (220)	538 (261)	9.13

IV. MODEL APPLICABILITY

It is necessary to verify the applicability of the proposed mathematical model before its application. This is done at both qualitative and quantitative levels based on BFs having a wide variety of inner volumes. First, the computer model has been used to study the effects of coke rate and hot blast rate on the performance of a 2000-m^3 BF with respect to productivity, top gas temperature, and top gas utilization factor, as well as the shape and position of cohesive zone (CZ), and the trends of the calculated results well agree with the general observations of BFs in practice.[36] Note that unless otherwise noted, CZ is defined according to the solid temperature range between 1473 K and 1673 K (1200 °C and 1400 °C) in simulations. Also, based on three online BFs, whose inner volumes are about 750 m^3 (one) and 5000 m^3 (two), quantitative comparisons between the calculated and measured results were made for the above-listed performance indicators, showing satisfactory agreement.[42,43]

Besides the global performance focused in the previous comparison, the in-furnace states are also considered in this study to further examine the validity of the present model. The recent experimental data obtained by Watakabe *et al.*[10] from the 9-m^3 LKAB experimental BF are taken for this purpose. The corresponding geometrical and operational conditions are listed in Tables III and IV, respectively. In the simulation, the burden distribution pattern at the BF top is derived from the measured CZ structures due to the lack of

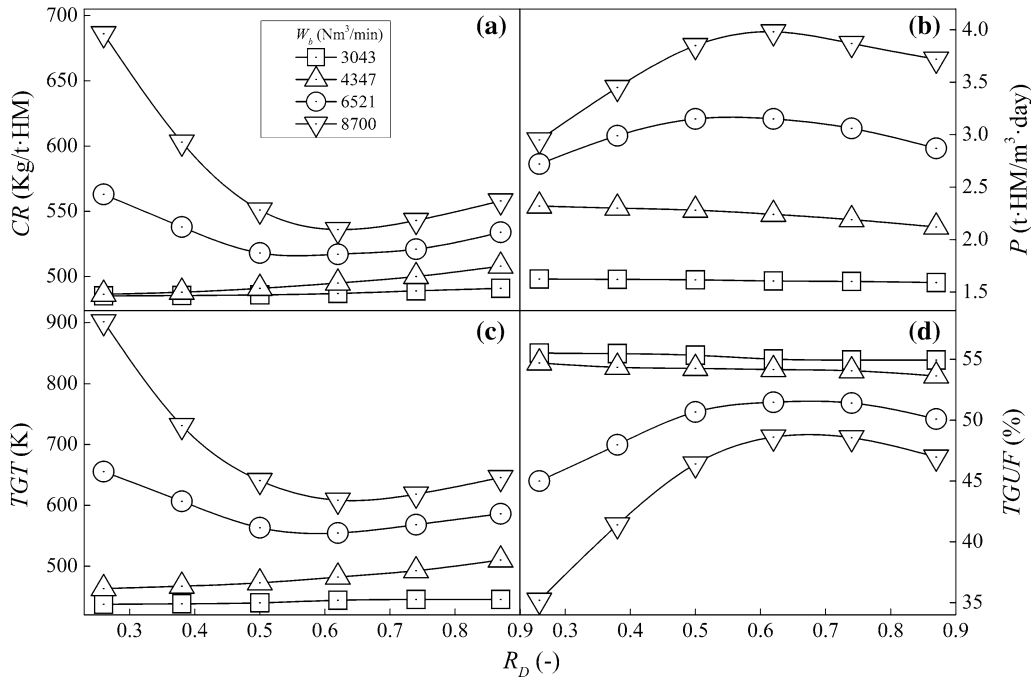

Fig. 3—Performance indicators as a function of R_D at different blast rates: (*a*) coke rate (*CR*), (*b*) productivity (*P*), (*c*) top gas temperature (*TGT*), and (*d*) utilization factor (*TGUF*).

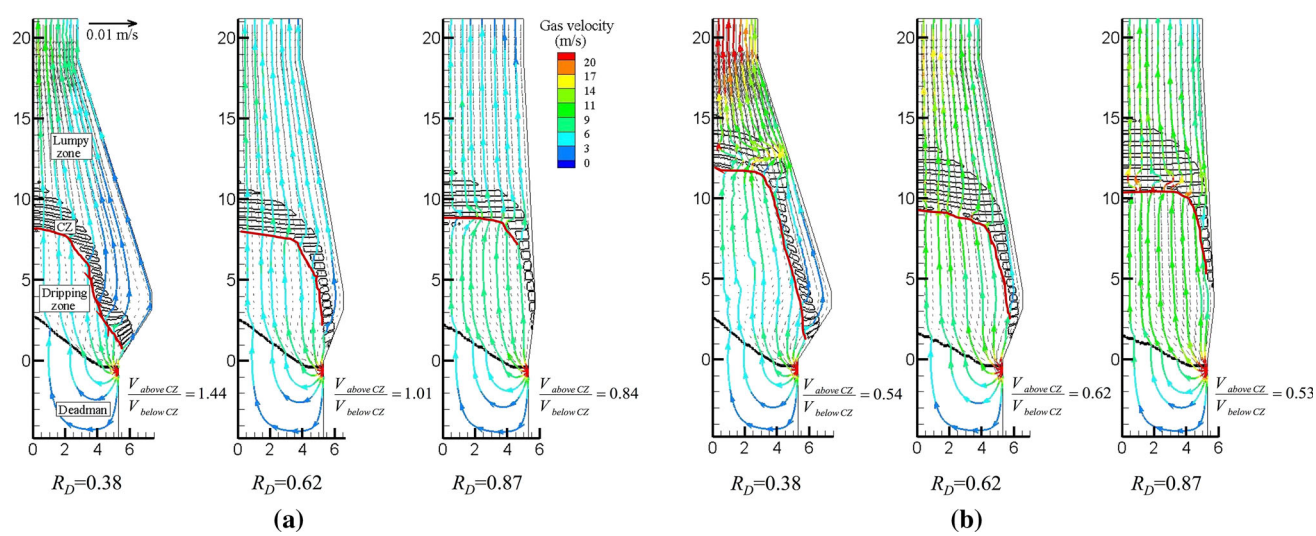

Fig. 4—Gas and solid flows inside different BFs operated at the blast rate of (*a*) 4347 Nm^3/min and (*b*) 8700 Nm^3/min.

experimental details. Figure 2(a) compares the CZs obtained from the experiments and simulations. In both studies, the CZs present an "inversed-V" shape in accordance to the so-called center-developed burden distribution pattern, as widely encountered in the BF practice. Overall, the model can satisfactorily re-produce the CZ shape and position. Figures 2(b) and (c) plot the radial profiles of calculated and measured gas temperature, respectively, at the upper and lower parts of the shaft. Expectedly, the temperature increases along the radial axis from the wall to the center at the two height levels considered, corresponding to the "inversed-V"-shaped CZ. The calculated and measured results reasonably agree with each other.

Figure 2(d) presents the axial variation of average reduction degree of ferrous materials. As seen from this figure, the reduction of ferrous materials proceeds at different rates in two regions: the relatively low temperature region where the reduction reactions are relatively slow, and the relatively high-temperature region where the reduction reactions take place in a faster manner. This is in line with our general understanding that

chemical reactions are faster when the reaction temperature is higher.[2] Again, the numerical and experimental results are in reasonably good agreement.

The comparison of the measured and calculated performance indicators is also performed for the LKAB BF and the results are given in Table V. Overall, the predictions are satisfactory with the errors less than 10 pct. It is noted that the top gas temperature is over predicted to some extent. This discrepancy may be due to the simplifications in formulating the model and in setting up the simulation conditions. Among them, the most possible reason may be that the physically and chemically combined water in burden materials is not considered in the present model. This water usually evaporates as long as burden materials are charged into BF, which lowers down the top gas temperature, but does not cause significant changes in the thermochemical phenomena inside a BF.[2] Nonetheless, all the results obtained thus far manifest that this process model can successfully predict the in-furnace states and global performance of BFs over a wide range of conditions, at least qualitatively.

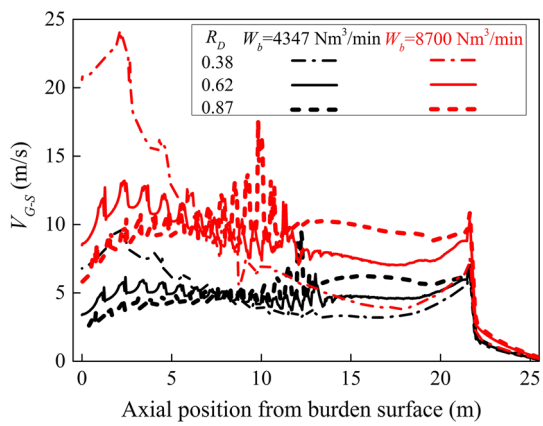

Fig. 5—Axial variation of gas-solid relative velocities inside different BFs operated at different blast rates.

V. RESULTS AND DISCUSSION

A. *Effect of Inner Profile on Global Performance*

To assess the furnace profiles at different productivities, the key performance indicators are first examined against blast rate, including coke rate, productivity, top gas temperature, and top gas utilization factor. The results are given in Figure 3. Note that varying blast rate aims to achieve operations at different productivities and the values of blast rate are pre-set based on the base furnace profile.

Figure 3(a) shows that with increasing R_D, the coke rate increases at relatively low blast rates, but rapidly decreases first to a minimum and then gradually increases at relatively high blast rates. A comprised optimum R_D can therefore be identified, at which the coke rates are relatively small at relatively low blast rates and presents minimum values at relatively high blast rates. It is equal to 0.62 under the present conditions. As such, the inner profile has much more complicated impacts on BF performance than those reported in the numerical work of Inada *et al.*,[35] who only observed the monotonous increase of fuel rate with the increase of R_D. This result also indicates that the

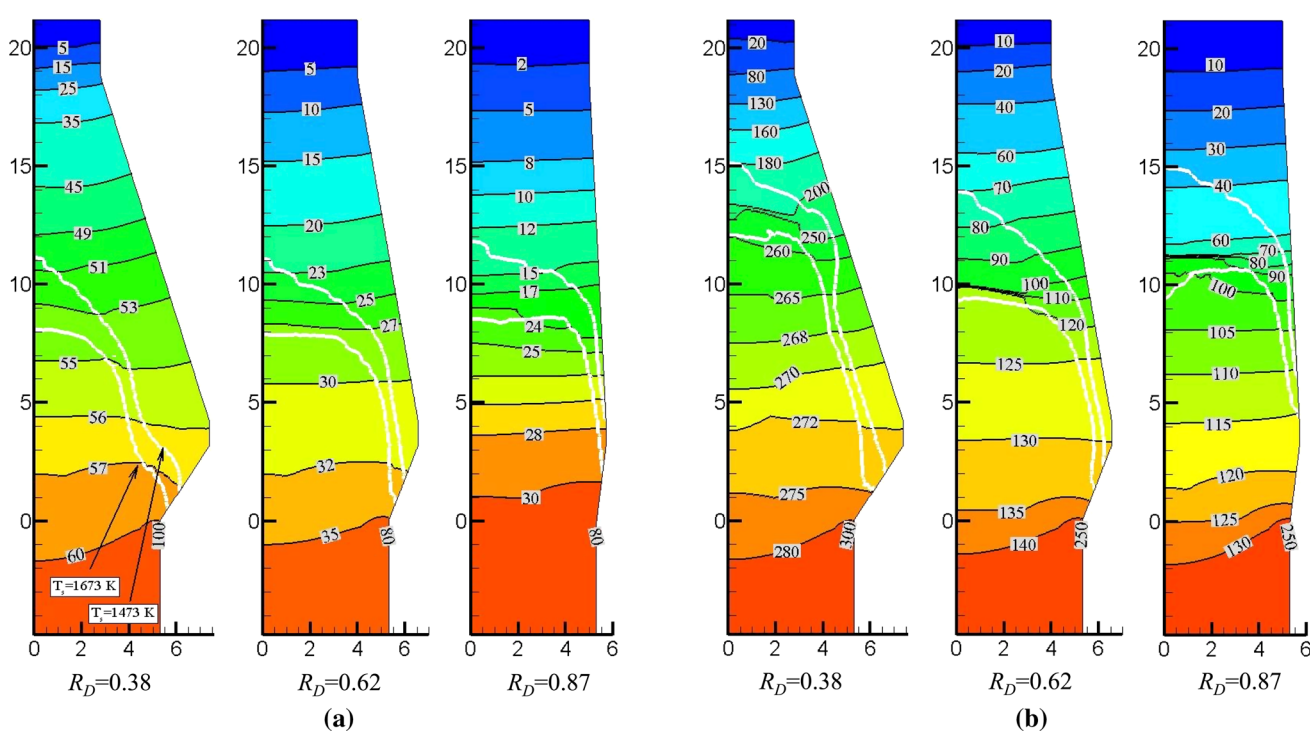

Fig. 6—Distributions of gas pressure inside different BFs operated at the blast rate of (*a*) 4347 Nm^3/min and (*b*) 8700 Nm^3/min.

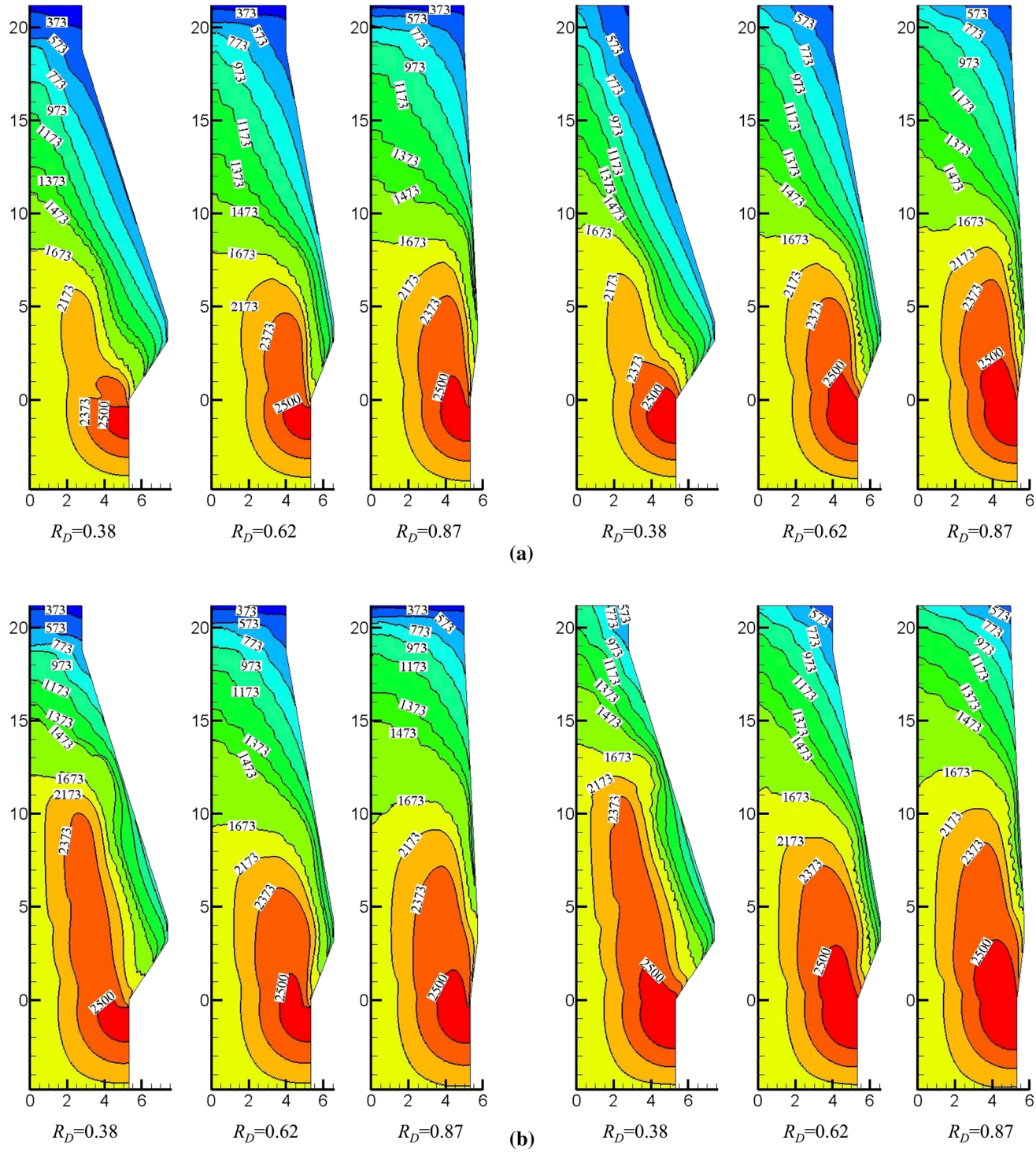

Fig. 7—Distributions of solid temperature (left) and gas temperature (right) inside different BFs operated at the blast rate of (*a*) 4347 Nm^3/min and (*b*) 8700 Nm^3/min.

variation of productivity should be considered in the BF design phase to be efficient and avoid the rapid change of process efficiency.

Figure 3(a) also shows that increasing blast rate generally increases the coke rate, to some extents. This result is in line with the experimental results obtained by different investigators.[2,37,38] It is of great interest to note that the change of coke rate is small at relatively low blast rates; however, it becomes significant at relatively high blast rates, in particular when R_D is too small. In other words, BF performance becomes very sensitive to BF profile when blast rate or productivity is

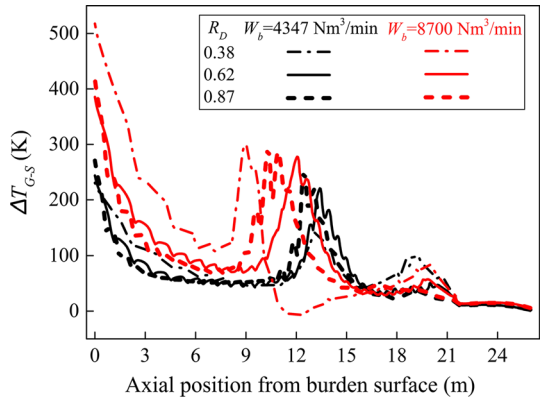

Fig. 8—Axial variations of gas-solid temperature difference inside different BFs operated at different blast rates.

relatively high. Additionally, the present study suggests that because the productivities of BFs with different volumes are often very different in practice, the predicted effect of BF volume on fuel rate by Inada *et al.*[34] at a fixed productivity should be the collective effects of BF geometry and productivity rather than that of geometry alone.

Figure 3(b) reveals the way productivity varies with inner profile at different blast rates. As seen from this figure, a higher blast rate expectedly leads to an increased productivity, because more oxygen is brought into the BF to combust with coke in the raceway to generate more energy to produce HM. This result is consistent with the intensified operation frequently encountered in the BF practice.[2,44] It can also be seen from Figure 3(b) that with increasing R_D, the productivity decreases at relatively low blast rates, whereas

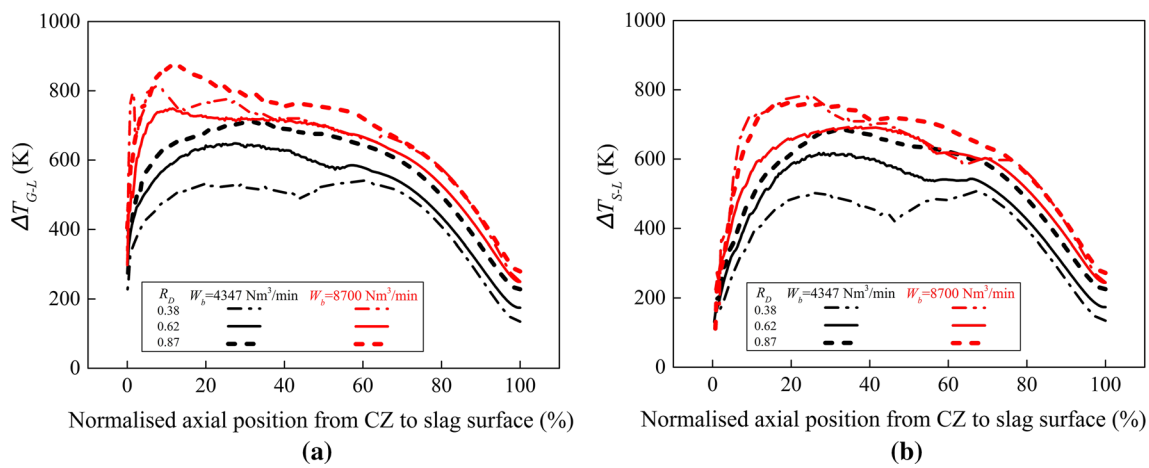

Fig. 9—Axial variations of temperature difference: (*a*) between gas and liquid phases and (*b*) between solid and liquid phases in the region below CZ.

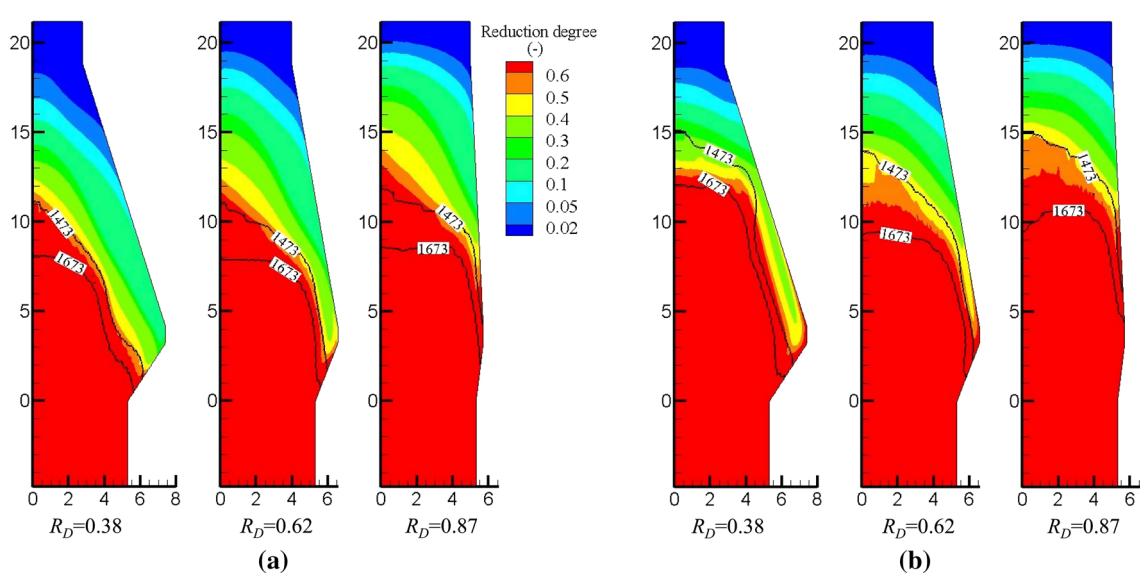

Fig. 10—Reduction degree in the region above CZ inside different BFs operated at the blast rate of (*a*) 4347 Nm³/min and (*b*) 8700 Nm³/min.

increases initially to a maximum and then decreases at relatively high blast rates. This trend is opposite to that of coke rate, because for a given blast rate, the thermal and chemical energy generated by the coke combustion in the raceway is the same, and their better utilization (corresponding to a lower coke rate) helps consume more ferrous materials to achieve an increased productivity. Note that for the purpose of intensified smelting, it is expected that productivity linearly increases with the increase of blast rate. This is, however, not achieved under the present conditions. It is especially the case for BFs with relatively small R_V, where the increase of productivity with blast rate is minor when the blast is too high.

Figures 3(c) and (d) present the variations of top gas temperature and top gas utilization factor with blast rate. These two performance indicators, respectively, reflect the thermal and chemical energy efficiency of hot reducing gas inside a BF. They are essentially linked with fuel rate. Under the present conditions, there are no injections of auxiliary fuels and the combustion of coke with hot blast is the primary energy source. A lower coke rate therefore corresponds to a better thermal and chemical energy efficiency and thus decreased energy requirements from the raceway. These relationships can be well reflected from Figures 3(a), (c), and (d), which show that a larger top gas utilization factor and a lower top gas temperature correspond to a lower coke rate at different R_D and blast rates.

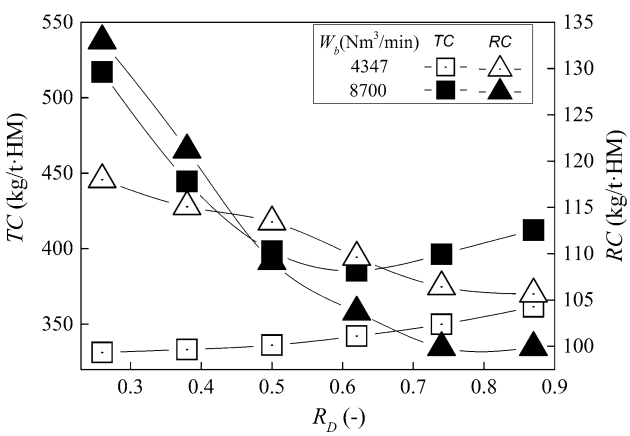

Fig. 11—Coke consumptions due to chemical reactions (*RC*) and combustion in front of tuyeres (*TC*) as a function of R_D at different blast rates.

Overall, Figure 3 reveals that at the optimum R_D, the variations of the energy-related performance indicators with blast rate such as coke rate, top gas utilization factor, and top gas temperature are the smallest; at the same time, the change of the productivity is largely in a linear manner. This result indicates that the optimum BF design helps realize intensified smelting operation while maintain a stable running state.

B. *Effect of Inner Profile on BF Inner States*

Process performance is governed by the in-furnace states such as flows and heat and mass transfer. Analysis of the in-furnace states can generate some insights into the flow and thermochemical behaviors inside a BF. It can hence provide a better understanding of process performance, as well as some useful information to guide BF design and operation. Such analysis is difficult to achieve experimentally or in practice but can be readily performed based on the numerical simulations. For clarity, the following analysis focuses on the representative results. However, the findings are qualitatively valid to other cases considered.

1. *Flow Behaviors*

Figure 4 shows the gas-solid flows inside BFs operated at different blast rates. Four zones can be identified, including lumpy zone, CZ, dripping zone, and deadman, as labeled in Figure 4(a) (R_D = 0.38). The main characteristics of the CZs largely control BF performance and are focused here. Generally, all of the CZs present an "inversed-V" shape under the present conditions, which suggests that the gas flow is reasonably developed

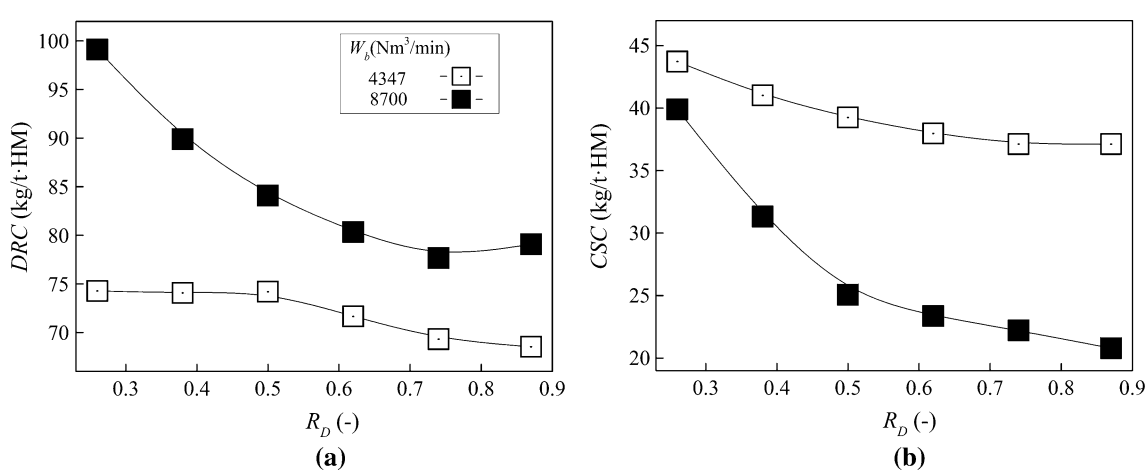

Fig. 12—Coke consumptions due to (*a*) direct reduction (DRC), and (*b*) carbon solution loss (CSC) as a function of R_D at different blast rates.

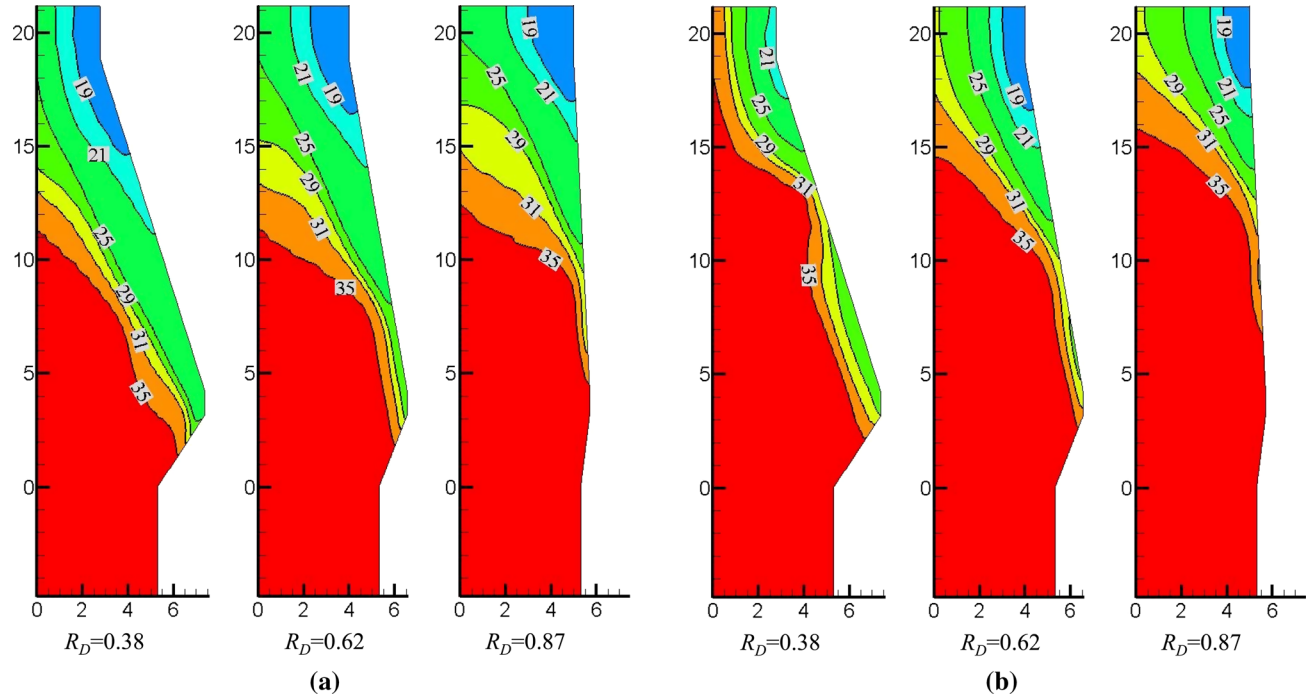

Fig. 13—CO concentration inside different BFs operated at the blast rate of (*a*) 4347 Nm^3/min and (*b*) 8700 Nm^3/min.

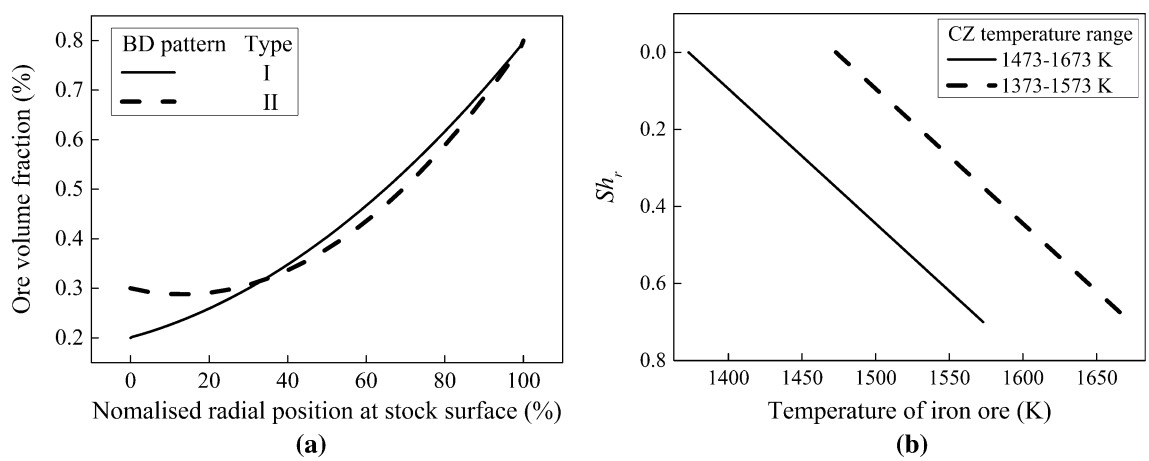

Fig. 14—Simulated burden distribution (BD) patterns at the BF top (*a*) and softening-melting temperature ranges of iron ore (*b*).

in the center region. As R_D increases, the CZ position rises at relatively low blast rates; however, it descends first and then rises at relatively high blast rates. These results can be quantitatively reflected from the volumetric ratio of the upper and lower regions demarcated by CZ, as given in Figure 4. Notably, the effective length of CZ (as highlighted by the red solid lines in Figure 4) is shortened with the increase of R_D or the decrease of blast rate. Here, the effective length is estimated according to the CZ parts, through coke slits of which the gas apparently flows upward. A longer effective CZ length suggests a stronger interaction between gas and CZ, and thus an increased resistance. In accordance to these CZ profiles, the gas flow is better developed near the wall region and becomes more uniform along the radial direction with increasing R_D. This is because the resistance of CZ and the distance allowing gas to flow upward are both reduced near the peripheral region.

To further understand the flows inside BFs, the relative velocities of gas to solid phases are examined and the results are given in Figure 5. Generally, a larger magnitude of relative velocity suggests a shortened contacting time between gas and solid phases and thus a deteriorated mass and heat transfer. Note that in Figure 5 (and Figures 8 and 9), the results are averaged over the radial direction. The relative velocities are generally larger at a higher blast rate because of the intensified downward solid flow and upward gas flow.

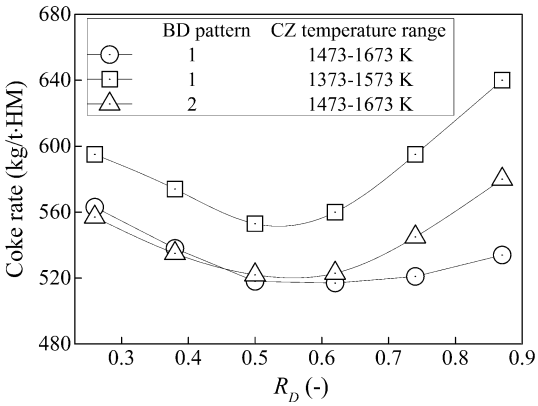

Fig. 15—Coke rates as a function of furnace profile at different burden distribution patterns and softening-melting temperature ranges for the blast rate of 6521 Nm^3/min.

When R_D increases for a given blast rate, the relative velocities increase in the lower part, but sharply decrease first and then slow down in the upper part. The sharp change of relative velocities becomes particularly obvious at small R_D, which can be explained as follows. The decreased lateral dimensions of the upper furnace for BFs with small R_D lead to large relative velocities there. This worsens the heat transfer from the gas phase to the solid phase, resulting in a relatively high gas temperature, which in turn causes gas expansion and increases gas-solid relative velocities. Furthermore, the worsened heat transfer requires more coke combusting in the raceway to provide adequate thermal and chemical energy for heating up and melting burden materials and sustaining reactions, which further increases the relative velocities.

Figure 6 shows that the distribution of gas pressure that indicates furnace permeability and gas resistance. As seen from this figure, the pressure rapidly drops when the gas flows through CZ due to the strong interactions of gas with the softening and melting ferrous materials there. Overall, the in-furnace gas pressure generally increases with the increase of blast rate due to the increased gas-solid relative velocities in the entire furnace, as shown in Figure 5. Conversely, increasing R_D leads to the decrease of gas pressure. This result may be due to two factors. One is the shortened effective length of CZ. Another is the decreased gas-solid relative velocities in the upper furnace.

2. *Thermal Behaviors*

Figures 7(a) and (b) show the distributions of solid and gas temperature. Their contour lines present similar profiles and the gas temperature is generally higher, which is in line with the field experience.[2] Corresponding to "inversed-V"-shaped CZs, both the solid and gas temperatures decrease along the radial direction from the center to the wall at the same height. The gas/solid temperature is observed to have a more uniform radial distribution with increasing R_D, which accounts for the flattened CZ in the radial direction. Furthermore, when R_D increases, the contour lines of gas or solid temperature in the zone above CZ consistently shift up at relatively low blast rates. However, they shift down initially and then shift up at relatively high blast rates.

Figure 8 shows the temperature difference between gas and solid phases along the axial direction. With increasing axial distance away from the burden surface to the slag surface, the gas-solid temperature difference rapidly drops and then slows down to approach to a constant at the slag surface. Along with this general variation, two peaks appear due to different combination effects of CZ, deadman, and dripping zones (see Figure 4), where the heat exchanges proceed differently. In a CZ, the heat exchange between gas and ferrous materials mainly occurs at the interface between ore and coke when ferrous materials are in the softening and melting state, and thus the efficiency is relatively low. This leads to large gas-solid temperature differences in CZ. This heat exchange can be enhanced in the deadman zone where the solid phase is nearly static and can be heated up to a more complete extent, leading to a small gas-solid temperature difference which has also been numerically and experimentally observed by Jin *et al.*[45] The co-existence of CZ and dripping zones at the same height level leads to the big peak. It is the deadman, CZ, and dripping zones that collectively cause the small peak. When R_D increases at a given blast rate, the curves of the gas-solid temperature difference in the region above CZ rapidly shift down first and then slow down, corresponding to the changes of the gas-solid relative velocities.

Figure 9 shows the gas-liquid and solid-liquid temperature differences. In this figure, the axial position is normalized by the maximum normal distance between the slag surface and the lower boundary of CZ where liquids are generated and start to flow downwards. The variations of the two temperature differences show similar trends due to the small gas-solid temperature difference, which is in line with the observations of Jin *et al.*[45] When the axial distance increases toward the slag surface, either the solid-liquid or gas-liquid temperature difference drastically increases initially to a maximum, and then decreases from gradually to rapidly. The increase of the temperature difference is caused by the heat sinks associated with the reduction of silicon dioxides and the direct reduction of wustite, as well as by the high temperature of gas coming from the tuyere. Furthermore, it is observed that with increasing R_D, the curves of gas/solid-liquid temperature difference shift up at relatively low blast rates. In contrast, they slightly shift down first and then shift up at relatively large blast rates.

The results in Figures 8 and 9 together reflect the thermal energy efficiency inside BFs against the considered furnace profiles and blast rates, to a large extent. Generally, a large temperature difference between gas and solid/liquid may lead to a high top gas temperature. For example, the larger gas/solid-liquid temperature difference suggests a low heat exchange efficiency in the zone below CZ. It requires more thermal energy from the raceway to heat the liquid to the target HM temperature, which may enhance top gas temperature. This understanding can also apply to the gas-solid temperature difference in the region above CZ. At

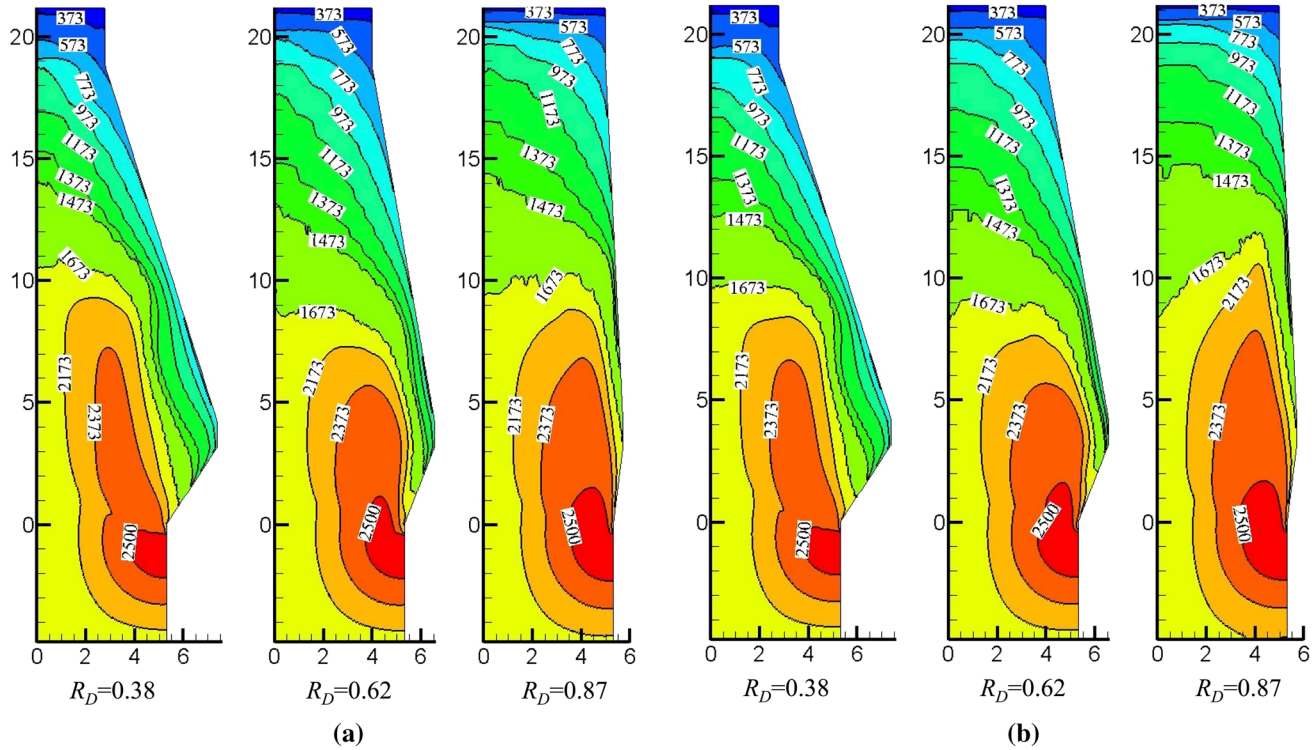

Fig. 16—Distribution of solid temperature within BFs operated with the burden distribution pattern of (*a*) type I and (*b*) type II, for blast rate of 6521 Nm^3/min.

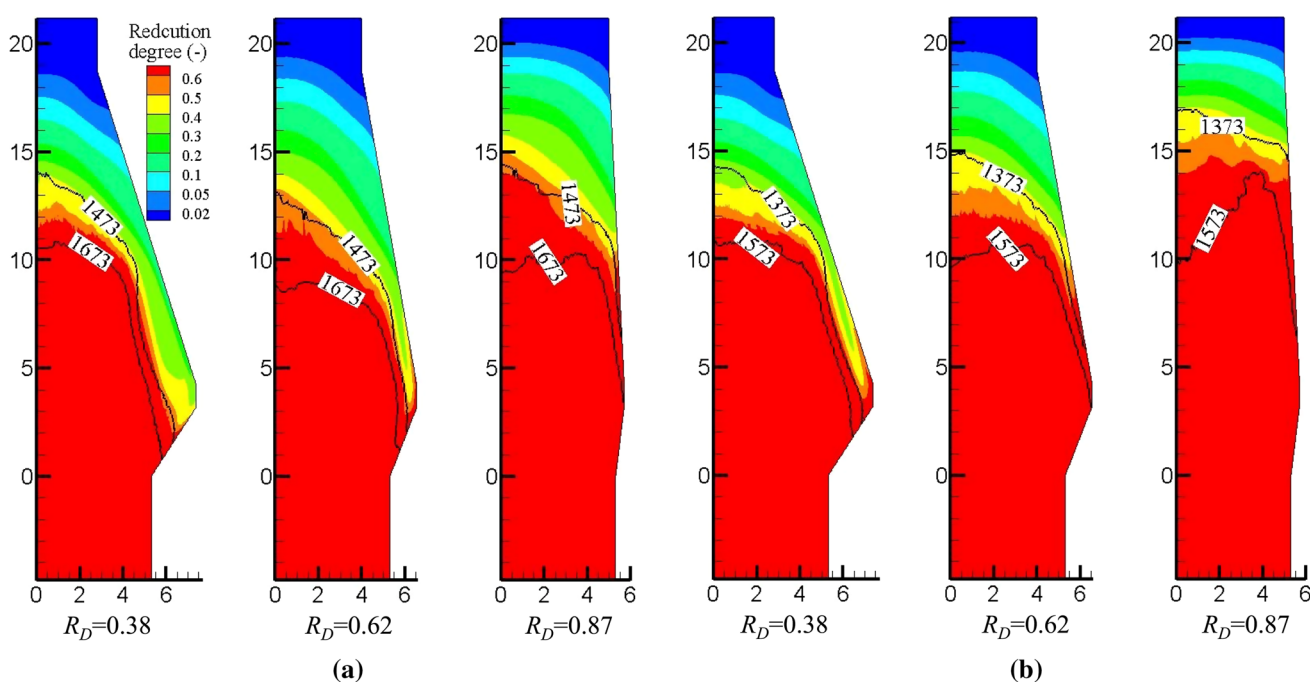

Fig. 17—Reduction degree within BFs charged with ferrous materials having softening-melting temperature range of (*a*) 1473 K through 1673 K (1200 °C through 1400 °C) and (*b*) 1373 K through 1573 K (1100 °C through 1300 °C), for the blast rate of 6521 Nm^3/min.

relatively low blast rates, the gas/solid-liquid temperature difference is much larger than that of gas-solid temperature difference, which plays a dominant role and accounts for the increased top gas temperature and fuel rate at larger R_D. Conversely, at relatively large blast rates, the dominant factor is gas-solid temperature difference at small R_D but again switches to the gas/solid-liquid temperature difference at larger R_D,

leading to the non-monotonous variation of top gas temperature and fuel rate with R_D.

3. *Coke Consumptions*

Figure 10 shows the spatial distributions of reduction degree of iron-bearing materials in the region above CZ inside the furnaces. This aims to demonstrate how the ferrous materials are reduced within the dry zone (*i.e.*, above CZ) where the indirect reduction mainly occurs. Note that it is established that the thermodynamics for the exothermic indirect reduction reactions are significantly deteriorated in the high-temperature region below CZ where the ferrous materials are reduced mainly *via* direct reduction that is strongly endothermic. Generally, with increasing blast rate or decreasing R_D, the reduction degree along the CZ top boundary [at the solid temperature of 1473 K (1200 °C)] decreases. This result suggests the indirect reduction process is delayed, which increases direct reduction and thus coke consumption.

Figure 11 plots the coke consumptions as a function of the furnace profiles and blast rates considered. The coke in a BF is consumed through (1) chemical reactions such as direct reduction of wustite and carbon solution loss, (2) combustion in the raceway, and (3) carburization. The amount of the last item is largely constant and thus not included in Figure 11. As seen from this figure, when R_D increases, the coke consumption due to the combustion in the raceway increases at relatively low blast rates. However, it drastically decreases first to a minimum and then increases at relatively high blast rates. Conversely, the coke consumption due to chemical reactions always decreases with the increase of R_D, because the increased lateral dimensions extend the gas-solid contacting time and facilitate indirect reduction. Moreover, it is of interest to note that the amount of coke reacted is more significant at relatively small R_D and relatively large blast rates. Note that the reactions directly consuming coke are strongly endothermic. Their massive occurrence requires more heat generated in the raceway to heat up HM to the target temperature. This result contributes to the large gas/solid-liquid temperature differences inside BFs with relatively small R_D while being operated at relatively large blast rates.

When blast rate is increased, two opposite effects are generated. On one hand, the thermal efficiency is deteriorated because of the increased relative velocities between gas and solid phases in the zone above CZ. This situation also leads to a shortened contacting time between gas and solid phases, and thus decreases indirect reduction (Figure 10). In other words, more coke is consumed through the direct reduction of ferrous materials at relatively large blast rates (Figure 12(a)). On the other hand, the reducing atmosphere inside the furnace becomes stronger with increasing blast rate, reflected by the increased CO concentration (Figure 13). Accordingly, the carbon solution loss reactions are suppressed, which reduces the coke consumptions by these reactions at relatively large blast rates (Figure 12(b)). Note that the intensified reducing atmosphere does not affect direct reduction of wustite within slag. Nonetheless, the coke consumption due to the direct reduction or carbon solution loss is very significant at relatively small R_D and relatively large blast rates (Figure 12).

VI. INTERACTION WITH OTHER FACTORS

Materials properties and burden charging operations may have a significant impact on BF performance and thus determination of BF geometry. The variables may interact with each other, giving complicated effects on BF performance. To confirm this, some efforts are also made in this respect, although dedicated studies are needed to generate comprehensive results in the future. Here, we consider two key factors: burden distribution pattern at the BF top and softening-melting temperature range of ferrous materials. Note that such information is the inputs of the model. Figure 14(a) shows the two burden distribution patterns: type I for all the above simulations and type II for the simulations in this section. Accordingly, the radial distribution of ore-to-coke ratio becomes more uniform. To consider the effect of material property, the softening-melting temperature range used to define CZ is changed from 1473 K through 1673 K (1200 °C through 1400 °C) to 1373 K through 1573 K (1100 °C through 1300 °C). The former range is used in all the above simulations. Figure 14(b) plots the softening-melting behaviors of ferrous materials in terms of shrinkage ratio (Sh_r) against solid temperature, corresponding to the two CZ regions defined by different temperature ranges.

Figure 15 reveals how the fuel rate varies with inner profile at different burden conditions. It is shown that despite the changes of the conditions, the optimum value of R_D does not change much, and is in the range of from 0.5 through 0.62. Notably, when the burden distribution pattern is changed from type I to type II, the fuel rate only becomes slightly lower at relatively small R_D, whereas much higher at relatively large R_D. Two reasons can account for the large increase of fuel rate at relatively large R_D when burden distribution becomes more uniform. First, the CZ apparently becomes thicker and higher, where the efficiency of the heat exchange between the gas and solid phases is relatively low (Figure 16). Second, the gas flow is less developed near the center region and stronger near the peripheral region, leading to more heat loss at the wall. Accordingly, more coke combusts to produce adequate thermal energy to achieve the target HM temperature through a longer-distance heating-up process.

Figure 15 also shows when the softening and melting temperature range is entirely lowered down by 100 K (−163 °C), the fuel rate generally increases and the extent is different for different inner profiles. To explain the result, the distribution of reduction degree is examined and the resulting results are given in Figure 17. When the softening-melting temperature decreases, the ferrous materials begin to be softened at an earlier stage. Consequently, the CZ position becomes higher, providing a longer distance for the heating-up process of liquids. The effect is, however, limited because of the relatively high productivities considered there. On the other hand, the indirect reduction process

is considerably delayed before entering the CZ, as reflected by the reduction degree at the top boundary of the CZ in Figure 17. Note that the thermodynamics of indirect reduction is dramatically deteriorated inside CZ. Consequently, direct reduction becomes more developed which are strongly endothermic and thus the liquids are more difficult to be heated up. As such, the fuel rate has to be increased to achieve the target HM temperature.

VII. CONCLUSIONS

The inner profile of ironmaking blast furnace can significantly affect the flow and heat and mass transfer and, in turn, the process performance. This effect may vary with operational and material conditions but has not been quantitatively examined. In this study, the in-furnace states and performance of BFs with different inner profiles are studied by a multi-fluid process model, with special reference to the effect of throat-to-belly diameter ratio at varying productivity and burden conditions. The major findings can be summarized as follows:

(1) The model proposed offers an effective method to study ironmaking blast furnace over a wide range of conditions. It can satisfactorily predict in-furnace states in terms of layered cohesive zone, gas temperature, and reduction degree as well as global performance indicators such as top gas temperature, top gas utilization factor, and productivity.
(2) When throat-to-belly diameter ratio (R_D) increases, the fuel rate increases at relatively low productivities; however, it initially decreases to a minimum and then increases at relatively high productivities. When R_D is too small, increasing productivity can drastically deteriorate the flow and thermochemical behaviors above cohesive zone, leading to the different variation trends of fuel rate.
(3) Optimum R_D can be identified with the relatively low fuel rate under the conditions considered. The optimum BF also has potential for maintaining stable operations over a wide range of conditions and facilitating intensified smelting operation.
(4) The effects of inner furnace are found sensitive to burden distribution and softening-melting temperature of ferrous materials. Material properties together with operational conditions therefore need to be considered case by case in determining BF profiles. The present model can be used for this purpose.

Finally, it should be pointed out in the BF practice, burden may experience obvious expansion and contraction with varying in-furnace thermal states due to the poor quality of raw materials and/or improper operations. Also, burden descent irregularity such as fluidization, channeling, and other unsmooth movements may occur at some local areas. Modeling of these phenomena should be useful to identify potential operation problems under different conditions but very challenging. In this respect, dedicated efforts are needed, and discrete approach, although still undergoing heavy developments for describing the BF ironmaking process, should be better than continuum approach.

ACKNOWLEDGMENTS

The authors are grateful to the Australian Research Council (ARC) and Central Iron & Steel Research Institute (CISRI) for the financial support of this work, and the National Computational Infrastructure (NCI) and Intersect Australia for the use of their high-performance computational facilities.

REFERENCES

1. I.F. Kurunov: *Metallurgist*, 2012, vol. 56, pp. 241–46.
2. A.K. Biswas: *Principles of Blast Furnace Ironmaking: Theory and Practice*, Cootha Publishing House, Brisbane, 1981.
3. M. Ichida, K. Anan, M. Takao, K. Kakiuchi, Y. Morizane, I. Yamada, and T. Nakayama: *Nippon Steel Tech. Rep.*, 2006, vol. 94, pp. 80–86.
4. M. Ichida, K. Tamura, Y. Okuno, K. Yamaguchi, M. Nakayama, and M. Nakamura: *Tetsu to Hagane*, 1992, vol. 78, pp. 58–65.
5. M. Shimizu, A. Yamaguchi, S. Inaba, and K. Narita: *Tetsu-to-Hagané*, 1982, vol. 68, pp. 936–45.
6. K. Narita, M. Shimizu and S. Inaba, Report of 54th Committe of Gakushin (Japan Socieety for Promotion of Science), Rport No. 1537, 1980.
7. X.F. Dong, A.B. Yu, J.I. Yagi, and P. Zulli: *ISIJ Int.*, 2007, vol. 47, pp. 1553–70.
8. H.P. Zhu, Z.Y. Zhou, R.Y. Yang, and A.B. Yu: *Chem. Eng. Sci.*, 2008, vol. 63, pp. 5728–70.
9. H.P. Zhu, Z.Y. Zhou, R.Y. Yang, and A.B. Yu: *Chem. Eng. Sci.*, 2007, vol. 62, pp. 3378–96.
10. S. Watakabe, K. Miyagawa, S. Matsuzaki, T. Inada, Y. Tomita, K. Saito, M. Osame, P. Sikstrom, L.S. Okvist, and J.O. Wikstrom: *ISIJ Int.*, 2013, vol. 53, pp. 2065–71.
11. T. Ariyama, S. Natsui, T. Kon, S. Ueda, S. Kikuchi, and H. Nogami: *ISIJ Int.*, 2014, vol. 54, pp. 1457–71.
12. S. Ueda, S. Natsui, H. Nogami, J. Yagi, and T. Ariyama: *ISIJ Int.*, 2010, vol. 50, pp. 914–23.
13. J. Yagi: *ISIJ Int.*, 1991, vol. 31, pp. 387–94.
14. Z.Y. Zhou, S.B. Kuang, K.W. Chu, and A.B. Yu: *J. Fluid Mech.*, 2010, vol. 661, pp. 482–510.
15. J.L. Zhang, Y.X. Chen, Z.Y. Fan, Z.W. Hu, T.J. Yang, and T. Ariyama: *J. Iron. Steel Res. Int.*, 2011, vol. 18, pp. 1–6.
16. T. Nouchi: Sato. M and K. Taakeda, The JFE Steel Corporation Steel Research Laboratory, Process analysis for blast furnaces by the discrete element method*JFE Technical Report*, 2009, vol. 33, pp. 28–33.
17. Z.Y. Fan, S. Igarashi, S. Natsui, S. Ueda, and T. Yang: R. Inoue and T AIryama*ISIJ Int.*, 2010, vol. 50, pp. 1406–12.
18. T. Umekage, M. Kadowaki, and S. Yuu: *ISIJ Int.*, 2007, vol. 47, pp. 659–68.
19. W.J. Yang, Z.Y. Zhou, and A.B. Yu: *Chem. Eng. J.*, 2015, vol. 278, pp. 339–52.
20. W.J. Yang, Z.Y. Zhou, D. Pinson, and A.B. Yu: *Metall. Mater. Trans. B*, 2014, vol. 46, pp. 977–92.
21. S. Natsui, R. Shibasaki, T. Kon, S. Ueda, R. Inoue, and T. Ariyama: *ISIJ Int.*, 2013, vol. 53, pp. 1770–78.
22. Z.Y. Zhou, H.P. Zhu, B. Wright, A.B. Yu, and P. Zulli: *Powder Technol.*, 2011, vol. 208, pp. 72–85.
23. P.R. Austin, H. Nogami, and J. Yagi: *ISIJ Int.*, 1997, vol. 37, pp. 748–55.
24. S.J. Chew, P. Zulli, and A.B. Yu: *ISIJ Int.*, 2001, vol. 41, pp. 1112–21.
25. S.J. Chew, P. Zulli, and A.B. Yu: *ISIJ Int.*, 2001, vol. 41, pp. 1122–30.

26. G.X. Wang, S.J. Chew, A.B. Yu, and P. Zulli: *Metall. Mater. Trans. B*, 1997, vol. 28, pp. 333–43.
27. K. Takatani, T. Inada, and Y. Ujisawa: *ISIJ Int.*, 1999, vol. 39, pp. 15–22.
28. S.J. Zhang, A.B. Yu, P. Zulli, B. Wright, and U. Tuzun: *ISIJ Int.*, 1998, vol. 38, pp. 1311–19.
29. D. Fu, Y. Chen, Y.F. Zhao, J. D'Alessio, K.J. Ferron, and C.Q. Zhou: *Appl. Therm. Eng.*, 2014, vol. 66, pp. 298–308.
30. K. Yang, S. Choi, J. Chung, and J. Yagi: *ISIJ Int.*, 2010, vol. 50, pp. 972–80.
31. X.F. Dong, A.B. Yu, S.J. Chew, and P. Zulli: *Metall. Mater. Trans. B*, 2010, vol. 41, pp. 330–49.
32. J.A. de Castro, A.J. da Silva, Y. Sasaki, and J. Yagi: *ISIJ Int.*, 2011, vol. 51, pp. 748–58.
33. P.R. Austin, H. Nogami, and J. Yagi: *ISIJ Int.*, 1997, vol. 37, pp. 458–67.
34. T. Inada, K. Takatani, K. Takata, and T. Yamamoto: *ISIJ Int.*, 2003, vol. 43, pp. 1143–50.
35. T. Inada, K. Takata, K. Takatani, and T. Yamamoto: *ISIJ Int.*, 2003, vol. 43, pp. 1003–10.
36. S.B. Kuang, Z.Y. Li, D.L. Yan, Y.H. Qi, and A.B. Yu: *Miner. Eng.*, 2014, vol. 63, pp. 45–56.
37. H.T. Brandi, G. Heynert, and H. Beer: *Stahl u. Eisen*, 1964, vol. 84, pp. 1169–74.
38. H. Beer and G. Heynert: *Stahl u. Eisen*, 1964, vol. 84, pp. 1353–65.
39. M.S. Chu, H. Nogami, and J. Yagi: *ISIJ Int.*, 2004, vol. 44, pp. 510–17.
40. M. Chu, H. Nogami, and J. Yagi: *ISIJ Int.*, 2004, vol. 44, pp. 801–08.
41. J.A. de Castro, H. Nogami, and J. Yagi: *ISIJ Int.*, 2001, vol. 41, pp. 18–24.
42. S.B. Kuang, Z. Y. Li and A. B. Yu, Model study of the optimization and investigation of burden distribution on Baosteel No 1 BF, Baosteel internal report, 2015.
43. S.B. Kuang, Z. Y. Li, S.D. Liu, J.Q. Gan and A. B. Yu, Modeling and optimization of 750-m^3 blast furnace in Baosteel, Baosteel internal report, 2015.
44. M. Geerdes, H. Toxopeus, and C. Van der Vliet: *Modern Blast Furnace Ironmaking: An Introduction*, IOS Press BV, Amsterdam, 2009.
45. H. Jin, S. Choi, J. Yagi, and J. Chung: *ISIJ Int.*, 2010, vol. 50, pp. 1023–31.
46. I. Muchi: *Trans. ISIJ*, 1967, vol. 7, pp. 223–37.
47. Y Omori: *Blast Furnace Phenomena and Modelling*, Elsevier, London, 1987.